FULL PAPER

Metasurfaces

ADVANCED
FUNCTIONAL
MATERIALS

www.afm-journal.d

Programmable Acoustic Metasurfaces

*Zhenhua Tian, Chen Shen, Junfei Li, Eric Reit, Yuyang Gu, Hai Fu,
Steven A. Cummer,* and Tony Jun Huang**

Metasurfaces open up unprecedented potential for wave engineering using subwavelength sheets. However, a severe limitation of current acoustic metasurfaces is their poor reconfigurability to achieve distinct functions on demand. Here a programmable acoustic metasurface that contains an array of tunable subwavelength unit cells to break the limitation and realize versatile two-dimensional wave manipulation functions is reported. Each unit cell of the metasurface is composed of a straight channel and five shunted Helmholtz resonators, whose effective mass can be tuned by a robust fluidic system. The phase and amplitude of acoustic waves transmitting through each unit cell can be modulated dynamically and continuously. Based on such mechanism, the metasurface is able to achieve versatile wave manipulation functions, by engineering the phase and amplitude of transmission waves in the subwavelength scale. Through acoustic field scanning experiments, multiple wave manipulation functions, including steering acoustic waves, engineering acoustic beams, and switching on/off acoustic energy flow by using one design of metasurface are visually demonstrated. This work extends the metasurface research and holds great potential for a wide range of applications including acoustic imaging, communication, levitation, and tweezers.

1. Introduction

Metasurfaces, as a two-dimensional (2D) equivalent of bulk metamaterials, have attracted numerous research efforts in recent years due to their powerful ability to control classical waves such as electromagnetic, acoustic, and elastic waves. In acoustics, metasurfaces offer a new paradigm for manipulating wave propagation,[1–4] engineering acoustic wavefront,[5–10] and realizing various interesting functions including acoustic cloaking,[11–13] holographic rendering,[14,15] and acoustic communication.[16,17] These functions are enabled by the fundamental subwavelength building blocks (unit cells) of

metasurfaces. When incoming acoustic waves fully interact with subwavelength unit cells, the phase and amplitude of reflected/transmitted waves will be modulated. Conventionally, most passive metasurfaces are designed of unit cells with fixed geometries, such as the space-coiling structures[18–20] and Helmholtz resonators.[21,22] Although they hold great potentials for acoustic wave manipulation, their acoustic responses cannot be tuned due to fixed geometries and their practical impacts are highly limited. Therefore, a programmable acoustic metasurface is desired, because its acoustic response can be modulated on demand to realize versatile functions.

Programmable metasurfaces have been proposed for manipulating electromagnetic and elastic waves.[23–26] However, the successful demonstration in acoustics has been scarce. To date, the most programmable acoustic metasurfaces still rely on actively controlled transducer arrays, which work in a similar way as the complex and expensive active phased arrays.[27,28] Acoustic metasurfaces purely based on passive materials/structures that are reconfigurable will avoid system complexity and offer low-cost solutions for practical applications. Recently, reconfigurable structures such as origami-inspired metamaterials[29] and elastomeric helices[30] have been demonstrated for manipulating acoustic waves. Resonant structures including Helmholtz resonators[31] and nanoelectromechanical metamaterials[32] have also been proposed to control acoustic and elastic waves. Given those reconfigurable structures are able to switch on/off acoustic energy flow, they still have limitations in continuously modulating the phase of acoustic waves and freely engineering the acoustic wavefront. Therefore, structure-based passive metasurfaces that can realize programmable modulation of both the acoustic phase and amplitude are advantageous for a wide range of applications, such as acoustic imaging, communication, levitation, and tweezers.

This study presents passive acoustic metasurfaces that are robustly programmable for realizing versatile wave manipulation functions, including steering acoustic waves, engineering acoustic beams, and switching on/off acoustic energy flow. The metasurface is composed of an array of tunable subwavelength unit cells. Each of them contains a straight channel and five shunted Helmholtz resonators, whose cavity sizes/effective mass can be tuned using a fluidic system. Moreover, the phase and amplitude of acoustic waves transmitting through each unit cell can be modulated dynamically and continuously.

Dr. Z. Tian, E. Reit, Y. Gu, H. Fu, Prof. T. J. Huang
Department of Mechanical Engineering and Materials Science
Duke University
Durham, NC 27708, USA
E-mail: tony.huang@duke.edu
Dr. C. Shen, J. Li, Prof. S. A. Cummer
Department of Electrical and Computer Engineering
Duke University
Durham, NC 27708, USA
E-mail: cummer@ee.duke.edu

ADVANCED
SCIENCE NEWS
www.advancedsciencenews.com

ADVANCED
FUNCTIONAL
MATERIALS
www.afm-journal.de

Based on such mechanism, the metasurface can achieve versatile 2D wave manipulation functions by engineering the transmission phase and amplitude in the subwavelength scale. We experimentally demonstrate that a metasurface can be programmed to realize multiple functions in a 2D waveguide, including steering acoustic waves, generating focused and tweezer-like acoustic beams, as well as guiding acoustic energy along a parabolic trajectory. In addition, we demonstrate that the metasurface can serve as a robust switch, whose ability goes beyond wavefront manipulation, for controlling acoustic energy flow and yielding high energy contrast in opposite directions.

2. Results

2.1. Mechanisms of the Programmable Acoustic Metasurface

Figure 1a shows a schematic diagram of the designed metasurface, which is composed of an array of tunable subwavelength unit cells. In this design, each unit cell can dynamically and continuously modulate the phase and amplitude of transmission acoustic waves at the subwavelength scale. Therefore, by properly engineering the acoustic modulation introduced by each subwavelength unit cell, the metasurface is able to control its acoustic response for realizing versatile 2D wave manipulation functions.

As shown in Figure 1b, a tunable unit cell is composed of a straight channel and five shunted Helmholtz resonators, which are loaded with fluid to modulate the cavity sizes (or effective mass) and acoustic responses. The dimensions of unit cells are $h = 21$ mm, $h_2 = 1$ mm, $h_3 = 2.5$ mm, $h_4 = 7$ mm, $w_1 = 6.2$ mm,

$w_2 = 1.5$ mm, and $w_3 = 1.8$ mm, as illustrated in Figure 1b. The width of each unit cell is 27.8 mm, which is approximately a quarter wavelength (28.6 mm) at the frequency of interest (3.0 kHz) to provide enough spatial resolution. The cavity size (or height h_1) of a resonator can be easily controlled by changing the fluid volume using a robust fluidic system. Since the acoustic impedance of water is much higher than that of air, it is used for this study. Figure 1c plots simulation results revealing the phase and amplitude of acoustic waves transmitting through a unit cell with respect to the cavity height h_1. On the one hand, when the cavity height increases from 0 to 14 mm, a full 2π span of phase change can be achieved at an operational frequency of 3.0 kHz. Meanwhile, the transmission amplitude is generally above 80%, ensuring high energy throughput. On the other hand, when the cavity height is above 18 mm, the transmission amplitude is nearly zero, which offers the potential to block acoustic waves using a metasurface. Based on these features, the proposed metasurface, which is composed of an array of tunable subwavelength unit cells, will be able to modulate its acoustic response at the subwavelength scale for realizing versatile wave manipulation functions, simply by changing the cavity sizes of shunted Helmholtz resonators (Figure 1d).

A single unit cell is first fabricated and experimentally tested to characterize its acoustic response during real-time modulation. The cavity sizes of shunted Helmholtz resonators are controlled by a pumping system with a flow rate of 0.5 mL s^{-1}. A loudspeaker sends Gaussian pulses to the unit cell and the transmitted acoustic waves are acquired by a microphone during the continuous changing of the pumping volume. The acquired acoustic signals in **Figure 2**a show the time of flight is gradually increasing with the increase of the volume pumped
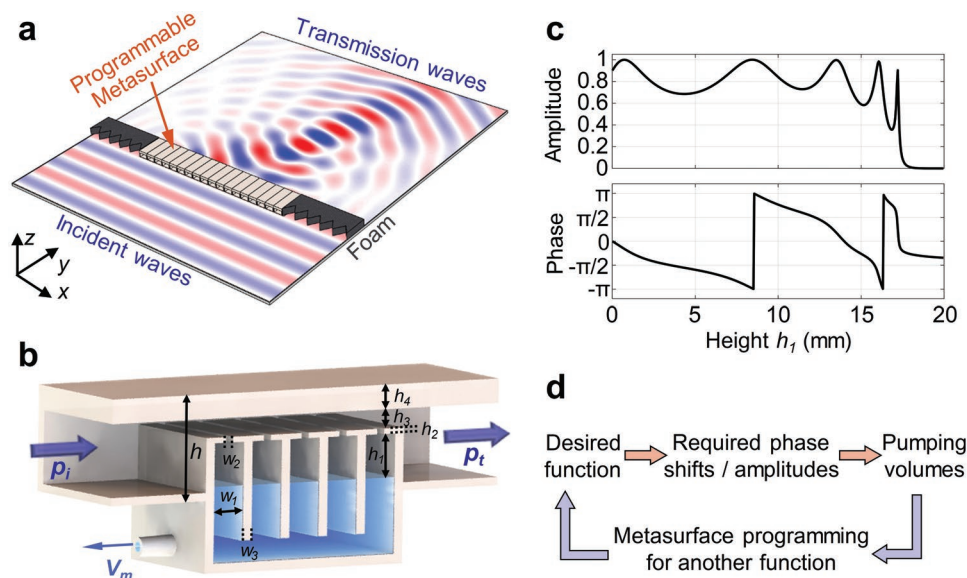

Figure 1. Mechanisms of programmable acoustic metasurfaces and characteristics of a tunable subwavelength unit cell. a) A schematic representation of the metasurface for manipulating acoustic waves. b) A schematic representation of a tunable subwavelength unit cell, which is composed of a straight channel and five shunted Helmholtz resonators. The cavity sizes are controlled by pumping fluid into/out of the unit cell. c) Numerical characterization of a unit cell. By changing the cavity height h_1, the acoustic phase can be tuned in the full range of $[-\pi, \pi]$ while maintaining high transmission amplitude. When the cavity height is over 18 mm, the transmission coefficient drops to zero. d) Procedures of modulating the metasurface to realize versatile functions.
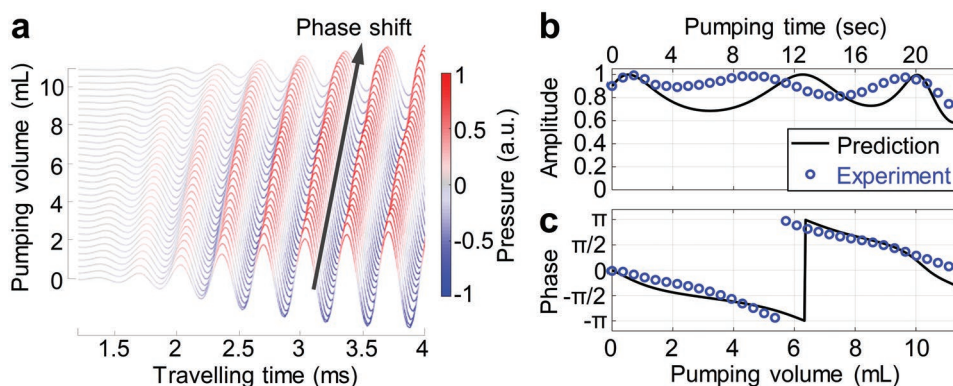
ADVANCED
SCIENCE NEWS
www.advancedsciencenews.com

ADVANCED
FUNCTIONAL
MATERIALS
www.afm-journal.de

Figure 2. Real-time modulation of a tunable unit cell. a) Evolution of acquired signals of transmitted waves with respect to the pumping volume. b) Amplitude and c) phase of transmitted waves with respect to the pumping volume. The pumping flow rate is 0.5 mL s^{-1}.

out of the unit cell, which confirms the capability of the tunable unit cell for modulating acoustic waves continuously and dynamically. For further characterization, Fourier transform is applied on the acquired signals to extract the amplitude and phase of transmitted waves. In Figure 2b, the discrepancies between amplitude relations obtained from the experiment and the numerical simulation could be attributed to experimental uncertainties, fabrication tolerance, and the thermoviscous effect[33] that is not considered in the simulation. Figure 2c shows a complete 2π phase modulation is achieved by gradually pumping 12 mL water out of the cavities in 24 s. In addition, the experimental phases agree well with predictions obtained from numerical simulations. The characterization results reveal that the developed fluid-actuated tunable unit cell can realize arbitrary phase modulation in a dynamic and continuous manner.

The developed tunable subwavelength unit cell has the merit of continuously modulating transmission phase from $-\pi$ to π as well as tuning the transmission coefficient from 0 to 1, by gradually changing the cavity sizes of Helmholtz resonators using a fluidic system. This merit lays the foundation for dynamically manipulating acoustic waves using our metasurface. Multiple functions can be easily realized through the reconfiguration of only one metasurface, whereas the traditional metasurfaces with fixed configurations require costly and time/labor-consuming redesigning and fabrication. In the followings, we demonstrate three useful dynamic functions using a fabricated metasurface, including on-demand wave steering, acoustic beam engineering, and on/off switching of acoustic energy flow.

2.2. Acoustic Wave Steering

Real-time steering of acoustic waves is one of the key functions required for acoustic imaging in medical diagnostics[34,35] as well as quantitative damage inspection in nondestructive evaluation.[36–39] By gradually steering acoustic waves to different directions like a radar, a scanning image can be generated for diagnosis. Previously, such steering function is mainly realized by complex phased array systems that require high-end and expensive equipment to independently control the firing

time/phase delay of each transducer in the phased array. Although metasurfaces have been demonstrated for changing the acoustic wave direction, they still have limitations in dynamic control of the wave direction, which is a crucial function required for real-world applications.

Here, we demonstrate on-demand acoustic wave steering using the designed metasurface placed in a 2D waveguide. When all the unit cells are set to the same phase shift of π, there is no steering effect and the transmission waves still propagate in the same direction as the incident waves, as shown by the measured pressure field (**Figure 3**c). The experimental pressure field is normalized to the pressure measured in an empty 2D waveguide without the metasurface. The overall transmission of the assembled metasurface is around 85%, which shows high transmission efficiency of the proposed metasurface. Based on the generalized Snell's law,[40] waves can be refracted by introducing a linear phase gradient to the metasurface. As shown in Figure 3d, the direction of transmission waves is steered to 70°, by changing the phase shifts to gradient values in Figure 3f within 24 s through the pumping system. The wave patterns in the experimental wavefield (Figure 3d) agrees well with those in the analytical prediction (Figure 3b), which means the steering angle can be precisely controlled. Our study proves the novel capability for on-demand acoustic wave steering in 2D space using the designed metasurface. Such capability will be very helpful for developing metasurface based acoustic imaging and damage inspection methods.

2.3. Acoustic Beam Engineering

Acoustic beams, such as focused, tweezer-like, and nonparaxial beams, are of interest for a wide range of applications including medical acoustic imaging,[34,35] nondestructive evaluation,[36–39] acoustic tweezers,[41–48] energy harvesting,[49] and wireless energy transfer.[50,51] Although acoustic beams can be generated using conventional passive metasurfaces, those metasurfaces with fixed configurations lack maneuverability in tuning and reshaping the acoustic beams, once they are designed and fabricated. Metasurfaces that can be reconfigured to generate various types of acoustic beams are highly advantageous, and
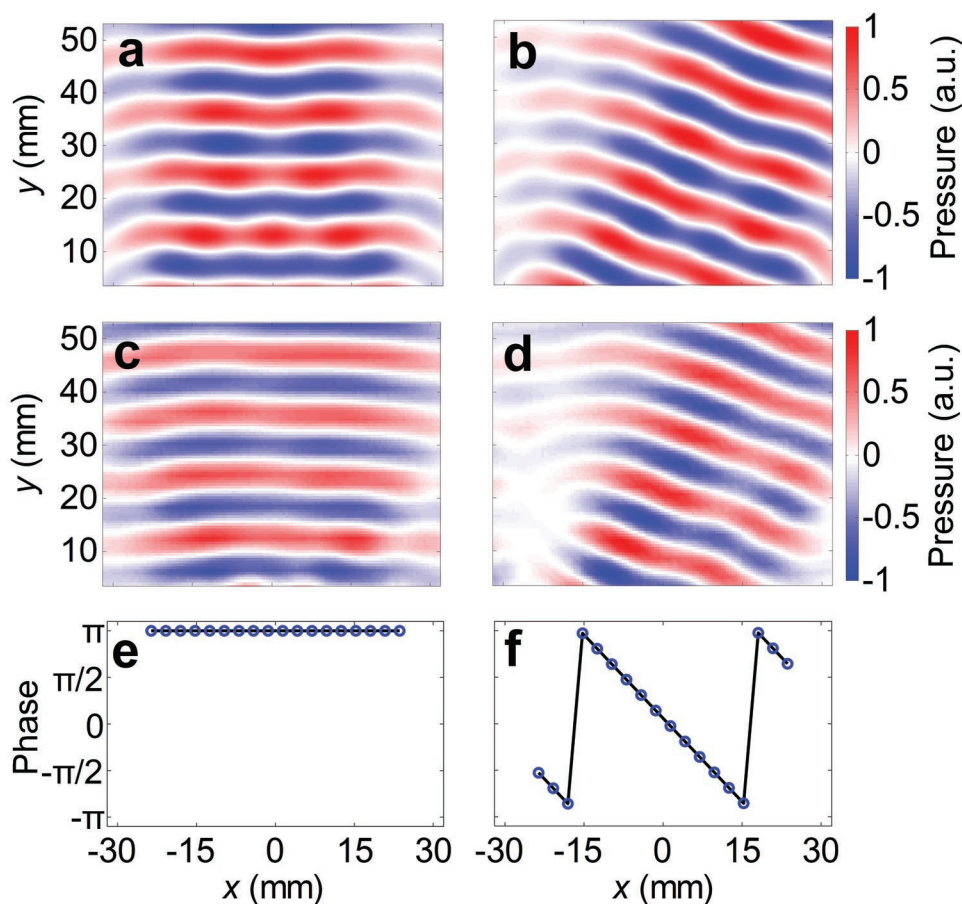
**ADVANCED
SCIENCE NEWS**
www.advancedsciencenews.com

**ADVANCED
FUNCTIONAL
MATERIALS**
www.afm-journal.de

Figure 3. Analytical and experimental results for acoustic wave steering. a) Analytical and c) experimental pressure fields without steering, when all the unit cells of the metasurface have the same phase shift given in (e). b) Analytical and d) experimental pressure fields showing the propagation direction is steered to 70°, when the unit cells have gradient phase shifts given in (f). The experimental pressure fields in (c) and (d) are normalized to the pressure measured in an empty 2D waveguide without the metasurface.

will enable multiple functions with one design and open more possibilities for the aforementioned applications.

Here, we experimentally demonstrate acoustic beam engineering with the developed metasurface in a 2D waveguide. By modulating the phase shifts, one metasurface can shape the acoustic energy field to various types of acoustic beams, such as focused, tweezer-like, and nonparaxial beams for different applications. Moreover, the beam features such as directions, focal point locations, and shapes can be readily tuned to adapt for different requirements.

Focusing acoustic energy to a narrow beam (beamforming) and dynamically steering the beam direction (beamsteering) are demonstrated as the first example. When phase shifts are set to values indicated in **Figure 4**k, a focused beam oriented in 90° with most energy confined in the region 17 mm away from the metasurface is generated (Figure 4f). Moreover, the beam features including both the focal distance and beam direction can be tuned by gradually changing the phase shifts. As shown in Figure 4g,h, the focal distance is increased to 24 mm and the beam direction is steered to 70°, respectively. The two functions, beamforming and beamsteering, demonstrated here will benefit multiple areas including acoustic imaging, energy harvesting, and wireless power transfer. For example, a focused beam with high energy confined in a narrow region will significantly improve the signal-to-noise ratio and resolution of acoustic imaging.[36,39]

In the second example, a focused beam is split into two halves along its central line, creating a new formation called a tweezer-like beam. Such transformation is enabled by introducing an additional phase shift of π to a half of the metasurface. Figure 4i shows a tweezer-like beam generated by changing the phase shifts to values indicated in Figure 4n, which have a phase difference of π between the left and right halves. The generated tweezer-like beam has zero energy in the center confined by a pair of symmetrically distributed bright lobes. Such tweezer-like beam is analogous to an acoustic trap[52] with a potential well along the central line of the beam. The tweezer-like beam generated by the metasurface can potentially be used for acoustic tweezers,[43–45] which have recently raised great interest for levitating objects,[53,54] rotating microorganisms,[55] patterning cells and microparticles,[56–59] as well as isolating cells and extracellular vesicles.[60–62]

As a third example, the acoustic energy field is shaped to a nonparaxial beam for guiding the acoustic energy along a desired convex trajectory. As shown in Figure 4j, a nonparaxial
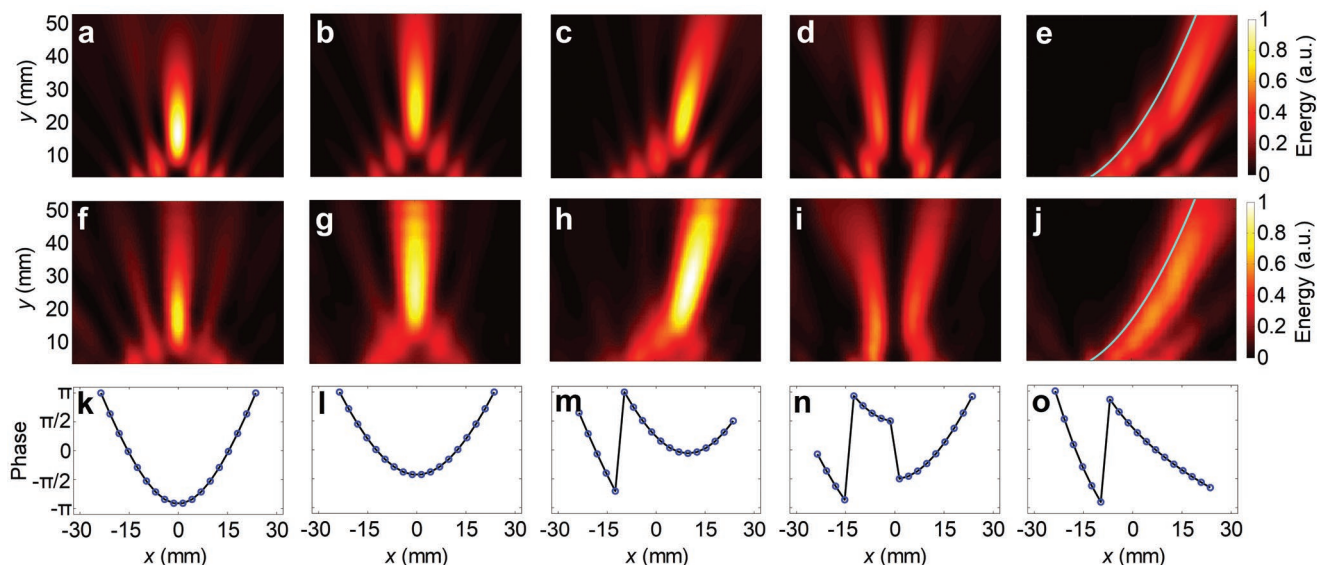
Figure 4. Analytical and experimental results for acoustic beam engineering. a–e) Analytical energy fields of five different acoustic beams, which demonstrate beamforming, tuning the focal distance, steering the beam direction, generating a tweezer-like beam, and guiding energy along a parabolic trajectory, respectively. f–j) Experimental energy fields and k–o) required phase shifts for the five acoustic beams. All the experimental energy fields agree well with the corresponding analytical predictions.

beam following a parabolic trajectory of $y = (x + 24)^2/35$ is generated, by changing the phase shifts to values indicated in Figure 4o. Such nonparaxial beam has the capability for circumventing obstacles and can potentially benefit acoustic imaging and therapeutic ultrasound. For example, in a complex structure with an obstacle, guiding the wave energy to bypass the obstacle is favorable to delivering more energy to the area of interest.

The three examples prove the unique capability of our acoustic metasurface for dynamic 2D beam engineering. The experimental results agree well with analytical predictions. Our design enables the generation of various types of acoustic beams as well as dynamically tuning the beam features via one metasurface, which surpasses the previous metasurfaces with fixed configurations. Beyond shaping the acoustic energy field to various beams, our acoustic metasurface may also be employed for transforming cylindrical waves to plane waves and creating a holographic rendering.

2.4. On/Off Switching of Acoustic Waves

Rapid and high-contrast on/off switching of acoustic energy flow is achieved by taking advantage of reversible amplitude modulation. When the cavities of shunted Helmholtz resonators are full of fluid, the cavity sizes are minimized and the transmission coefficient is nearly at the maximum as shown in Figure 1d. Therefore, by filling all the cavities of the metasurface with fluid, an on state with high acoustic energy is realized (**Figure 5**a). On the other hand, when the cavities are increased to their maximum allowable sizes, the shunted Helmholtz resonators nearly approach their resonance frequencies and the transmission coefficient is close to zero as shown in Figure 1d. Therefore, by emptying all the cavities of the metasurface, an off state with low acoustic energy transmission is realized (Figure 5b). For our current design, the switching time from one state to the other is nearly 30 s, which is limited by the large cavity size and the low flow rate of the pumping system.
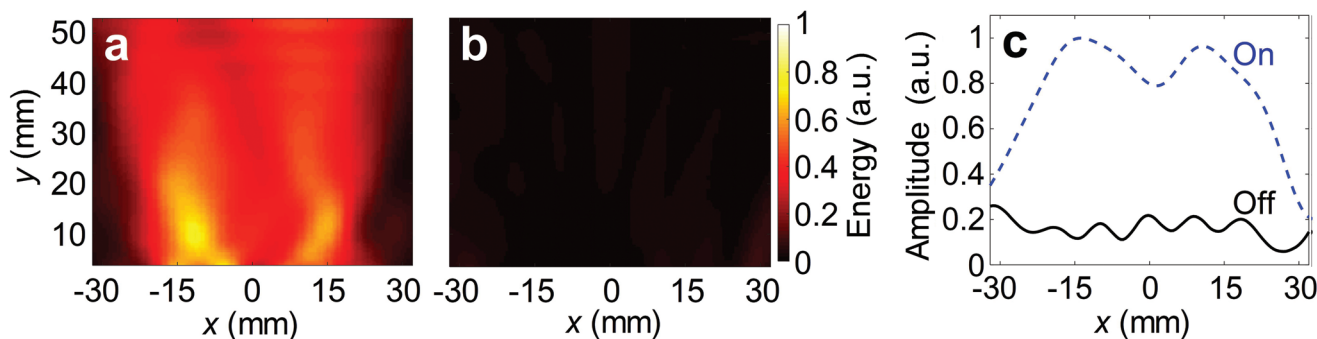

Figure 5. Experimental results for on/off switching of acoustic energy flow. Acoustic energy fields at a) on and b) off states. c) Comparison of pressure amplitudes along a line at $y = 25$ mm between on and off states.

In the future, we will optimize the metasurface and pumping system to realize a faster switching rate.

To evaluate the switching performance, pressure amplitudes along a line $y = 25$ mm at on and off states are compared in Figure 5c. After switching from on to off, the sound level drops nearly 16 dB in the region of [−20, 20] mm. It is also worth noting that such switching can be realized automatically. Our design expands the abilities of existing acoustic metasurfaces as well as provides a new paradigm for automatic switching of acoustic energy flow. Compared to previous switches,[29,30] our design has a much simpler configuration and can be readily implemented without changing the waveguide shape.

3. Discussion

In this study, we have designed, fabricated and experimentally demonstrated a passive acoustic metasurface composed of tunable subwavelength unit cells for programming acoustic waves and realizing versatile wave manipulation functions. By gradually changing the cavity sizes/effective mass of shunted Helmholtz resonators with a robust fluidic system, the subwavelength unit cell can continuously and dynamically modulate the phase and amplitude of transmission acoustic waves. With this merit, the developed acoustic metasurface is able to control its acoustic response and modulate acoustic waves in the subwavelength scale for achieving versatile wave manipulation functions. By experimentally scanning the acoustic pressure and energy fields modulated with a metasurface, we visually demonstrate multiple wave manipulation functions including steering plane waves, generating focused and tweezer-like acoustic beams, guiding acoustic waves along a parabolic trajectory, and switching on/off acoustic energy flow.

Previously, to realize distinct wave manipulation functions using passive metasurfaces made of fixed-geometry space-coiling structures[18–20] and Helmholtz resonators,[21,22] different metasurfaces need to be designed and fabricated through costly and time/labor consuming procedures. Moreover, their acoustic responses cannot be tuned on demand, once they are fabricated. Compared to the previous passive metasurfaces, our metasurface composed of tunable unit cells allows for on-demand control of its acoustic response and manipulation of acoustic wave propagation in versatile ways. Our metasurface also enables tunable functions such as steering the wave direction and changing the focal distance. Compared to some recently developed reconfigurable passive structures that have limitations in continuously modulating the acoustic phase and engineering the acoustic wavefront such as such as origami-inspired metamaterials[29] and elastomeric helices,[30] our metasurface breaks these limitations and thus enables more interesting functions including engineering acoustic beams and guiding waves along a parabolic trajectory, which usually require sophisticated phase/wavefront engineering. Another advantage over those recently developed reconfigurable structures is that our metasurface does not alter the direct physical path (the top straight channel) for air flow and light transmission.

This study extends metasurface research and takes a critical step forward toward metasurface based dynamic and multifunctional acoustic wave manipulation. With further improvements, our design concept can lead to many other unique capabilities. For example, the tunable unit cells can be bianisotropic[10] or holey structured[15] to achieve highly efficient wavefront manipulation or decoupled modulation of acoustic amplitude and phase. The tunable unit cells can also be assembled in 2D arrays for full three-dimensional (3D) manipulation of acoustic waves. In addition, if the switching rate of the metasurface is sufficiently high, the time-multiplexed beamforming[63,64] can be introduced to the metasurface. We expect the proposed programmable metasurfaces can be used for various applications including acoustic imaging, communication, levitation, and tweezers, as well as the scenarios that require smart and tunable properties.

4. Experimental Section

Fabrication of Acoustic Metasurfaces: The unit cells were fabricated by 3D polyjet printing (J750, Stratasys, US) with photopolymers (VeroClear, Stratasys, US) that have similar material properties as acrylics and much higher acoustic impedance than that of air. A metasurface was assembled with the fabricated unit cells that were distributed in a linear array with a period of 27.8 mm. The cavity sizes of shunted Helmholtz resonators in the metasurface were controlled by pumping water into/out of the resonators with automated multimodule syringe pumps (Cetoni, Nemesys, Germany).

Numerical Simulations: The numerical simulations of a unit cell were performed using the commercial finite element analysis software COMSOL Multiphysics with the Pressure Acoustics module. The background medium is air with density and speed of sound being 1.2 kg m^{-3} and 343 m s^{-1}, respectively. The air–water interface is modeled by an impedance boundary with density and speed of sound being 1000 kg m^{-3} and 1480 m s^{-1}, respectively. The walls of the unit cell are assumed to be rigid. To extract the transmission coefficients of the unit cell, a plane wave is incident from one side of the unit cell and perfectly matched layers are added to the other side to reduce reflections. A probe is placed in the outlet of the straight channel to extract the transmission amplitude at different cavity sizes.

Analytical Simulations: To efficiently predict the acoustic pressure and energy fields of transmission waves through a metasurface composed of subwavelength unit cells, an analytical model is developed. The detailed derivations of the analytical model are given in the Supporting Information. Based on the analytical model, a Matlab code is developed to simulate the acoustic pressure and energy fields given in Figures 3 and 4.

Phase Shifts for Wave Manipulation: By engineering the local phase shifts of all the subwavelength unit cells, the metasurface can shape the acoustic pressure and energy fields to versatile distributions. The input phased shifts for acoustic wave steering as well as generation of focused, tweezer-like, and nonparaxial acoustic beams are given in Figures 3 and 4. The derivations of phase shifts can be found in the Supporting Information.

Acoustic Wavefield Acquisition: The acoustic wavefield acquisition was performed in a 2D acoustic waveguide with a height of 21 mm. The experimental setup is given in Figure S1 of the Supporting Information. An array of 28 speakers was used to generate plane waves normally incident to the metasurface. The transmission acoustic waves were measured by a microphone attached on a 2D scanning system. The received acoustic signals were averaged four times to reduce the noise level. Through point-by-point scanning in an area of 65 × 55 cm^2 with a step of 2 cm, 2D wavefields of the transmission acoustic waves were acquired.

Supporting Information

Supporting Information is available from the Wiley Online Library or from the author.

Acknowledgements

Conflict of Interest

The authors declare no conflict of interest.

Keywords

[1] S. A. Cummer, J. Christensen, A. Alu, *Nat. Rev. Mater.* **2016**, *1*, 16001.

[2] G. C. Ma, P. Sheng, *Sci. Adv.* **2016**, *2*, e1501595.

[3] H. Ge, M. Yang, C. Ma, M. H. Lu, Y. F. Chen, N. Fang, P. Sheng, *Natl. Sci. Rev.* **2018**, *5*, 159.

[4] B. Assouar, B. Liang, Y. Wu, Y. Li, J.-C. Cheng, Y. Jing, *Nat. Rev. Mater.* **2018**, *3*, 460.

[5] Y. B. Xie, W. Q. Wang, H. Y. Chen, A. Konneker, B. I. Popa, S. A. Cummer, *Nat. Commun.* **2014**, *5*, 5553.

[6] K. Tang, C. Y. Qiu, M. Z. Ke, J. Y. Lu, Y. T. Ye, Z. Y. Liu, *Sci. Rep.* **2015**, *4*, 6517.

[7] J. Mei, Y. Wu, *New J. Phys.* **2014**, *16*, 123007.

[8] S. Koo, C. Cho, J. H. Jeong, N. Park, *Nat. Commun.* **2016**, *7*, 13012.

[9] G. Memoli, M. Caleap, M. Asakawa, D. R. Sahoo, B. W. Drinkwater, S. Subramanian, *Nat. Commun.* **2017**, *8*, 14608.

[10] J. F. Li, C. Shen, A. Diaz-Rubio, S. A. Tretyakov, S. A. Cummer, *Nat. Commun.* **2018**, *9*, 1342.

[11] C. Faure, O. Richoux, S. Felix, V. Pagneux, *Appl. Phys. Lett.* **2016**, *108*, 064103.

[12] H. Esfahlani, S. Karkar, H. Lissek, J. R. Mosig, *Phys. Rev. B* **2016**, *94*, 014302.

[13] Y. H. Yang, H. P. Wang, F. X. Yu, Z. W. Xu, H. S. Chen, *Sci. Rep.* **2016**, *6*, 20219.

[14] Y. B. Xie, C. Shen, W. Q. Wang, J. F. Li, D. J. Suo, B. I. Popa, Y. Jing, S. A. Cummer, *Sci. Rep.* **2016**, *6*, 35437.

[15] Y. F. Zhu, J. Hu, X. D. Fan, J. Yang, B. Liang, X. F. Zhu, J. C. Cheng, *Nat. Commun.* **2018**, *9*, 1632.

[16] C. Z. Shi, M. Dubois, Y. Wang, X. Zhang, *Proc. Natl. Acad. Sci. USA* **2017**, *114*, 7250.

[17] X. Jiang, B. Liang, J. C. Cheng, C. W. Qiu, *Adv. Mater.* **2018**, *30*, 1800257.

[18] Z. X. Liang, J. S. Li, *Phys. Rev. Lett.* **2012**, *108*, 114301.

[19] R. Ghaffarivardavagh, J. Nikolajczyk, R. G. Holt, S. Anderson, X. Zhang, *Nat. Commun.* **2018**, *9*, 1349.

[20] X. Ni, Y. Wu, Z. G. Chen, L. Y. Zheng, Y. L. Xu, P. Nayar, X. P. Liu, M. H. Lu, Y. F. Chen, *Sci. Rep.* **2015**, *4*, 7038.

[21] Y. Li, X. Jiang, B. Liang, J. C. Cheng, L. K. Zhang, *Phys. Rev. Appl.* **2015**, *4*, 024003.

[22] Y. Li, S. Qi, M. B. Assouar, *New J. Phys.* **2016**, *18*, 043024.

[23] T. J. Cui, M. Q. Qi, X. Wan, J. Zhao, Q. Cheng, *Light: Sci. Appl.* **2014**, *3*, e218.

[24] Q. Wang, E. T. F. Rogers, B. Gholipour, C. M. Wang, G. H. Yuan, J. H. Teng, N. I. Zheludev, *Nat. Photonics* **2016**, *10*, 60.

[25] K. Chen, Y. J. Feng, F. Monticone, J. M. Zhao, B. Zhu, T. Jiang, L. Zhang, Y. Kim, X. M. Ding, S. Zhang, A. Alu, C. W. Qiu, *Adv. Mater.* **2017**, *29*, 1606422.

[26] O. R. Bilal, A. Foehr, C. Daraio, *Adv. Mater.* **2017**, *29*, 1700628.

[27] W. Akl, A. Baz, *J. Vib. Acoust.* **2013**, *135*, 031001.

[28] B. I. Popa, D. Shinde, A. Konneker, S. A. Cummer, *Phys. Rev. B* **2015**, *91*, 220303.

[29] S. Babaee, J. T. B. Overvelde, E. R. Chen, V. Tournat, K. Bertoldi, *Sci. Adv.* **2016**, *2*, e1601019.

[30] S. Babaee, N. Viard, P. Wang, N. X. Fang, K. Bertoldi, *Adv. Mater.* **2016**, *28*, 1631.

[31] J. M. De Bedout, M. A. Franchek, R. J. Bernhard, L. Mongeau, *J. Sound Vib.* **1997**, *202*, 109.

[32] J. Cha, K. W. Kim, C. Daraio, *Nature* **2018**, *564*, 229.

[33] X. Jiang, Y. Li, L. Zhang, *J. Acoust. Soc. Am.* **2017**, *141*, EL363.

[34] J. A. Jensen, *Prog. Biophys. Mol. Biol.* **2007**, *93*, 153.

[35] E. Mace, G. Montaldo, I. Cohen, M. Baulac, M. Fink, M. Tanter, *Nat. Methods* **2011**, *8*, 662.

[36] V. Giurgiutiu, J. Bao, *Struct. Health Monit.: Int. J.* **2004**, *3*, 121.

[37] B. W. Drinkwater, P. D. Wilcox, *NDT&E Int.* **2006**, *39*, 525.

[38] A. Leleux, P. Micheau, M. Castaings, *J. Nondestr. Eval.* **2013**, *32*, 200.

[39] L. Y. Yu, Z. H. Tian, *Ultrasonics* **2016**, *68*, 43.

[40] N. F. Yu, P. Genevet, M. A. Kats, F. Aieta, J. P. Tetienne, F. Capasso, Z. Gaburro, *Science* **2011**, *334*, 333.

[41] A. Ozcelik, J. Rufo, F. Guo, Y. Gu, P. Li, J. Lata, T. J. Huang, *Nat. Methods* **2018**, *15*, 1021.

[42] S. P. Zhang, J. Lata, C. Chen, J. Mai, F. Guo, Z. Tian, L. Ren, Z. Mao, P. H. Huang, P. Li, S. Yang, T. J. Huang, *Nat. Commun.* **2018**, *9*, 2928.

[43] V. Marx, *Nat. Methods* **2015**, *12*, 41.

[44] J. Dual, T. Schwarz, *Lab Chip* **2012**, *12*, 244.

[45] J. Friend, L. Y. Yeo, *Rev. Mod. Phys.* **2011**, *83*, 647.

[46] X. Y. Ding, P. Li, S. C. S. Lin, Z. S. Stratton, N. Nama, F. Guo, D. Slotcavage, X. L. Mao, J. J. Shi, F. Costanzo, T. J. Huang, *Lab Chip* **2013**, *13*, 3626.

[47] W. Connacher, N. Q. Zhang, A. Huang, J. Y. Mei, S. Zhang, T. Gopesh, J. Friend, *Lab Chip* **2018**, *18*, 1952.

[48] Y. Bian, F. Guo, S. Yang, Z. Mao, H. Bachman, S. Y. Tang, L. Ren, B. Zhang, J. Gong, X. Guo, T. J. Huang, *Microfluidics Nanofluidics* **2017**, *21*, 132.

[49] S. Tol, F. L. Degertekin, A. Erturk, *Appl. Phys. Lett.* **2017**, *111*, 013503.

[50] S. Shahab, A. Erturk, *Smart Mater. Struct.* **2014**, *23*, 125032.

[51] S. Tol, Y. Xia, M. Ruzzene, A. Erturk, *Appl. Phys. Lett.* **2017**, *110*, 163505.

[52] F. Guo, Z. M. Mao, Y. C. Chen, Z. W. Xie, J. P. Lata, P. Li, L. Q. Ren, J. Y. Liu, J. Yang, M. Dao, S. Suresh, T. J. Huang, *Proc. Natl. Acad. Sci. USA* **2016**, *113*, 1522.

[53] D. Foresti, M. Nabavi, M. Klingauf, A. Ferrari, D. Poulikakos, *Proc. Natl. Acad. Sci. USA* **2013**, *110*, 12549.

[54] A. Marzo, S. A. Seah, B. W. Drinkwater, D. R. Sahoo, B. Long, S. Subramanian, *Nat. Commun.* **2015**, *6*, 8661.

**ADVANCED
SCIENCE NEWS**

www.advancedsciencenews.com

**ADVANCED
FUNCTIONAL
MATERIALS**

www.afm-journal.de

[55] X. Y. Ding, S. C. S. Lin, B. Kiraly, H. J. Yue, S. X. Li, I. K. Chiang, J. J. Shi, S. J. Benkovic, T. J. Huang, *Proc. Natl. Acad. Sci. USA* **2012**, *109*, 11105.

[56] S. Oberti, A. Neild, J. Dual, *J. Acoust. Soc. Am.* **2007**, *121*, 778.

[57] D. J. Collins, B. Morahan, J. Garcia-Bustos, C. Doerig, M. Plebanski, A. Neild, *Nat. Commun.* **2015**, *6*, 8686.

[58] F. Guo, P. Li, J. B. French, Z. M. Mao, H. Zhao, S. X. Li, N. Nama, J. R. Fick, S. J. Benkovic, T. J. Huang, *Proc. Natl. Acad. Sci. USA* **2015**, *112*, 43.

[59] K. Melde, A. G. Mark, T. Qiu, P. Fischer, *Nature* **2016**, *537*, 518.

[60] P. Li, Z. M. Mao, Z. L. Peng, L. L. Zhou, Y. C. Chen, P. H. Huang, C. I. Truica, J. J. Drabick, W. S. El-Deiry, M. Dao, S. Suresh, T. J. Huang, *Proc. Natl. Acad. Sci. USA* **2015**, *112*, 4970.

[61] M. X. Wu, Y. S. Ouyang, Z. Y. Wang, R. Zhang, P. H. Huang, C. Y. Chen, H. Li, P. Li, D. Quinn, M. Dao, S. Suresh, Y. Sadovsky, T. J. Huang, *Proc. Natl. Acad. Sci. USA* **2017**, *114*, 10584.

[62] L. Ren, S. Yang, P. Zhang, Z. Qu, Z. Mao, P. H. Huang, Y. Chen, M. Wu, L. Wang, P. Li, T. J. Huang, *Small* **2018**, *14*, 1801996.

[63] A. Marzo, M. Caleap, B. W. Drinkwater, *Phys. Rev. Lett.* **2018**, *120*, 044301.

[64] E. Zastrow, S. C. Hagness, B. D. Van Veen, J. E. Medow, *IEEE Trans. Biomed. Eng.* **2011**, *58*, 1574.

1808489 (8 of 8)